Supporting Information

Theoretical Insights into the Catalytic Mechanisms of $LiNi_{1/3}Co_{1/3}Mn_{1/3}O_2$ Cathode Surface in Diverse Ethylene Carbonate Decomposition Reactions

Mingyu Su[a], Dongsen Wu[b], Fanghua Ning[b, *], Yixue Wu[a], Yiming Guo[b], Huiying Zhang[b], Jin Yi[b], Dianxue Cao[a], Kai Zhu[a, *]

Author address

[a] Key Laboratory of Superlight Materials and Surface Technology (Ministry of Education), College of Material Science and Chemical Engineering, Harbin Engineering University, Harbin 150001, China

[b] Institute for Sustainable Energy/Department of Chemistry, College of Sciences, Shanghai University, Shanghai 200444, China

* Corresponding author.

E-mail: fhning@shu.edu.cn (Fanghua Ning); kzhu@hrbeu.edu.cn (Kai. Zhu)

Tables and Figures:

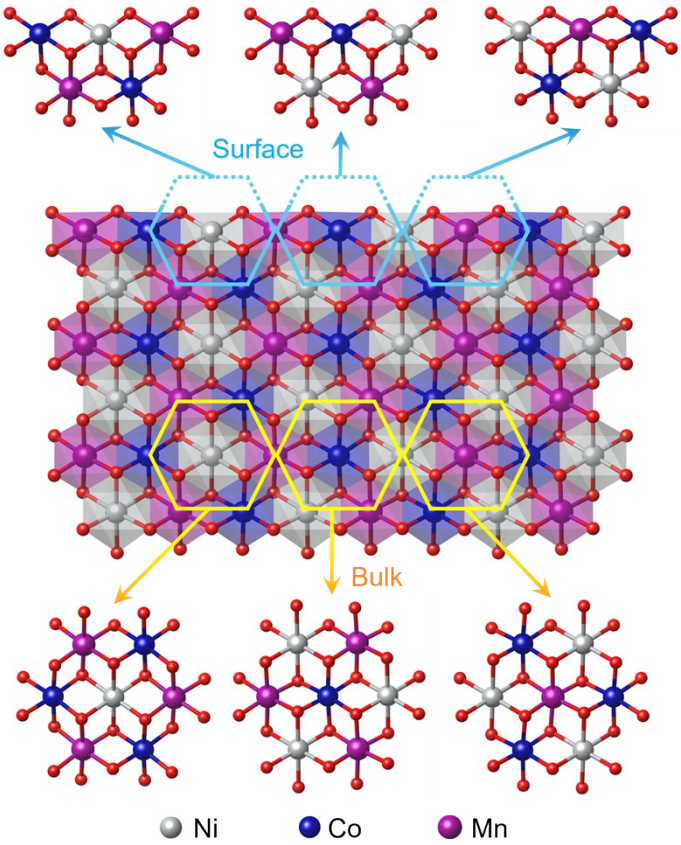

Figure S1 Schematic diagram of the local environment of Ni, Co and Mn on the surface and in the bulk of the positive electrode.

Table S1 The energy of $Li_{1/3}$NCMO (104) at 1 × 1 × 1, 2 × 2 × 1 and 3 × 3 × 1 k-point meshes.

K-point	Energy (eV)
1 × 1 × 1	-792.1259
2 × 2 × 1	-792.1040
3 × 3 × 1	-792.0894

Table S2 The adsorption energy (in eV) of EC at Ni, Co, and Mn sites on the $Li_{1/3}$NCMO (104) surface calculated with 1 × 1 × 1, 2 × 2 × 1 and 3 × 3 × 1 k-point meshes.

Active site / K-point	Co*	Ni*	Mn*
1 × 1 × 1	-0.0762	-0.1240	-0.2101
2 × 2 × 1	-0.0904	-0.0993	-0.1824
3 × 3 × 1	-0.0919	-0.0988	-0.1819

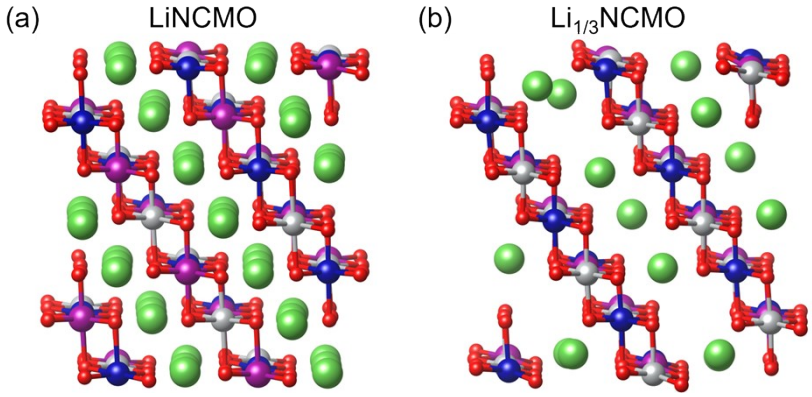

Figure S2 Structural schematic diagrams of the (104) slab model of LiNCMO (a) and $Li_{1/3}$NCMO (b).

Table S3 The magnetic moment and valence state of Co, Mn, and Ni ions at the surface and center sites of the LiNCMO slab system.

Region	Co		Mn		Ni	
	Magnetic moment	Valence state	Magnetic moment	Valence state	Magnetic moment	Valence state
Surface	-2.03 -2.05 0.03 0.00	5-coordinated Co^{3+}	3.92 3.91 3.29 3.28	5-coordinated Mn^{3+}	0.95 -0.91 1.68 1.69	5-coordinated Ni^{3+}
Bulk	0.02 0.02 0.02 0.02 0.03 0.02 0.00 0.01 2.08 2.10	6-coordinated Co^{3+}	3.28 3.28 3.28 3.29 3.28 3.28 3.28 3.27 3.93 3.92	6-coordinated Mn^{4+}	1.69 1.69 1.69 1.69 1.69 1.69 1.69 1.68 0.95 0.95	6-coordinated Ni^{2+}

Table S4 The magnetic moment and valence state of Co, Mn, and Ni ions at the surface and center sites of the $Li_{1/3}$NCMO slab system.

Region	Co		Mn		Ni	
	Magnetic moment	Valence state	Magnetic moment	Valence state	Magnetic moment	Valence state
Surface	2.55 2.57 0.03 0.04	5-coordinated Co^{3+}	3.48 3.49 3.26 3.27	5-coordinated Mn^{3+}	0.93 0.91 0.06 0.05	5-coordinated Ni^{3+}
Bulk	0.04 0.05 0.05 0.05 0.04 0.04 0.05 0.06 2.49	6-coordinated Co^{3+}	3.29 3.30 3.29 3.29 3.30 3.30 3.30 3.27 3.49	6-coordinated Mn^{4+}	0.07 0.08 0.07 0.07 0.07 0.08 0.09 0.05 -0.81	6-coordinated Ni^{2+}

-2.48	3.45	-0.88

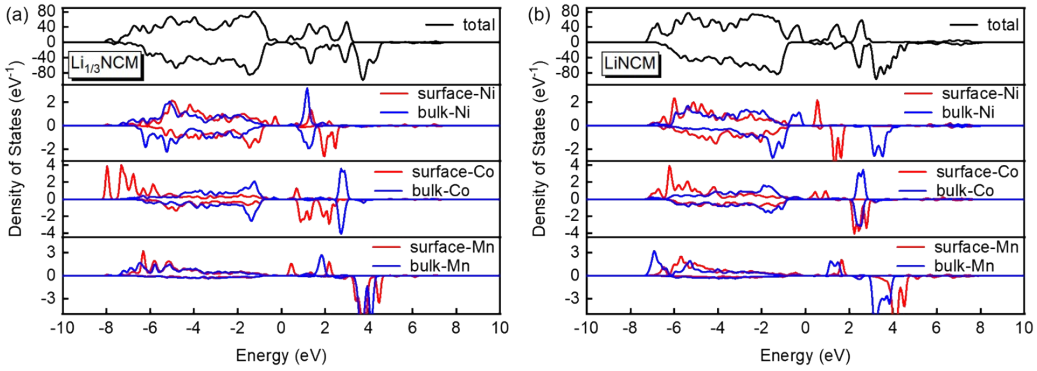

Figure S3 Total density of states (TDOS) and projected density of states (PDOS) of Ni, Co, and Mn on the surface and in the center of the LiNCMO (a) and $Li_{1/3}$NCMO (b) cathode.

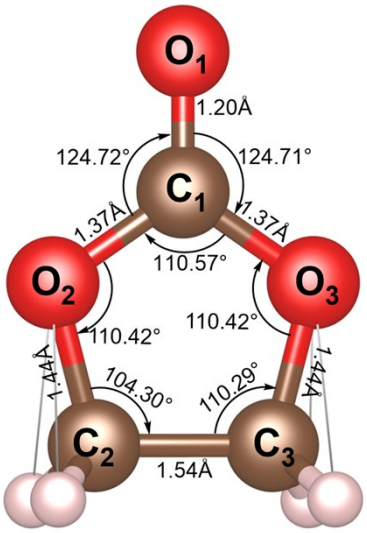

Figure S4 Geometric structure of the EC molecule.

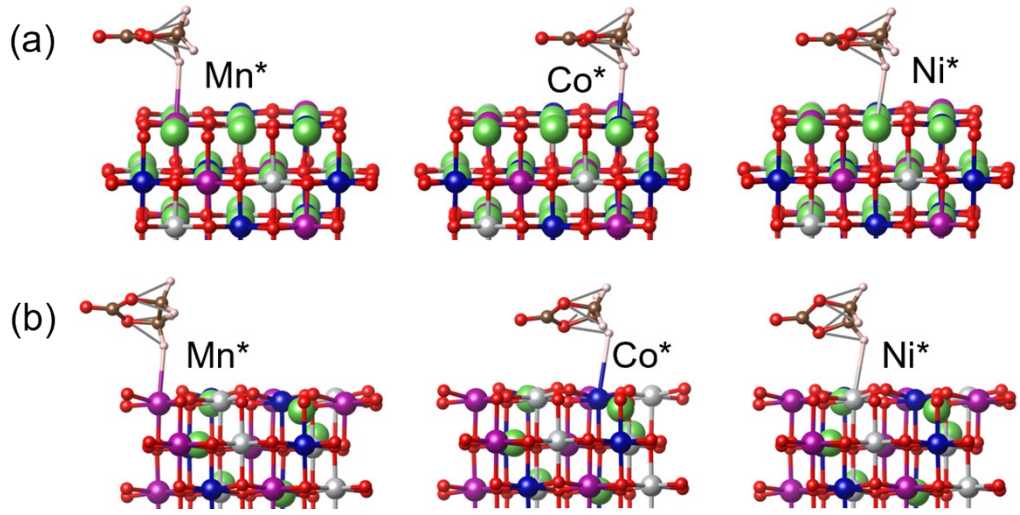

Figure S5 Schematic diagram of the top-η^1(H) adsorption configuration for EC adsorbed on three transition metal active sites of the LiNCMO (a) and $Li_{1/3}$NCMO (b) surfaces.

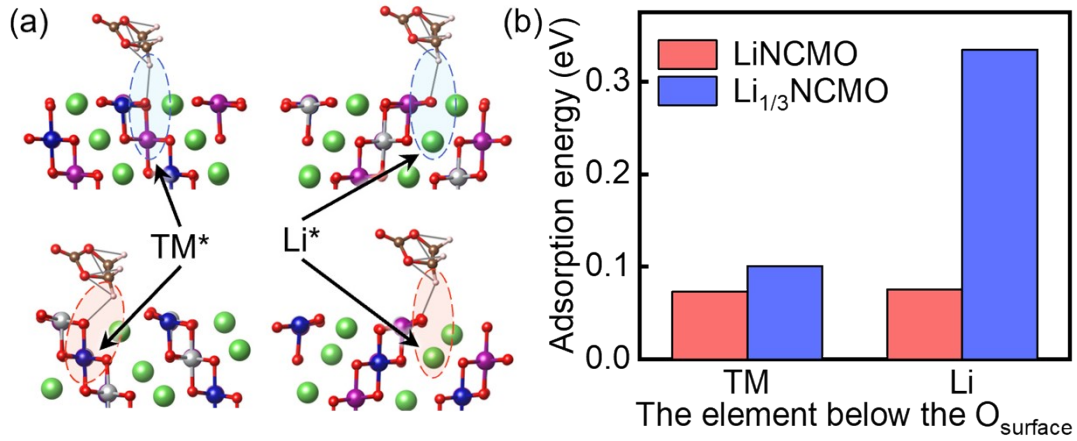

Figure S6 Schematic diagram (a) and adsorption energy (b) of the top-η^1(H) adsorption configuration for EC absorbed on oxygen sites of the cathode surfaces.

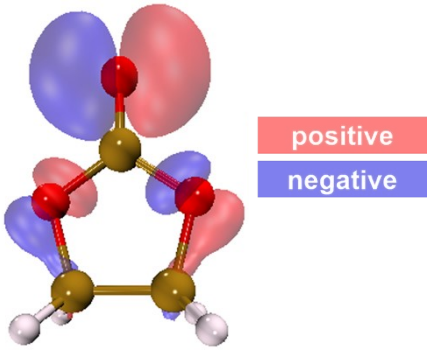

Figure S7 The HOMO charge distribution of EC molecule.

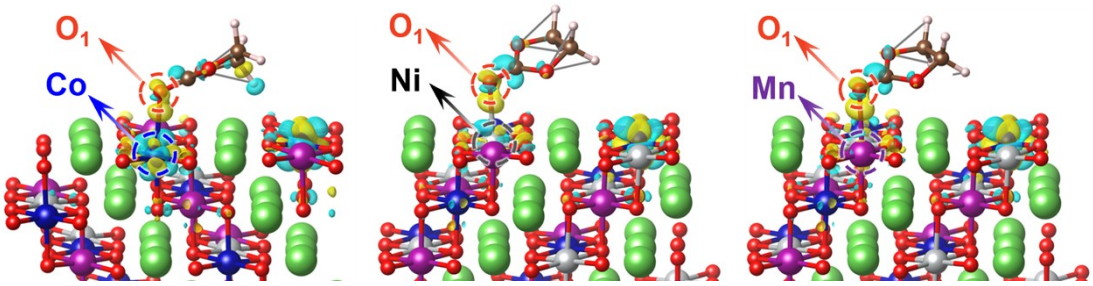

Figure S8 Charge density difference upon the adsorption of EC on LiNCMO.

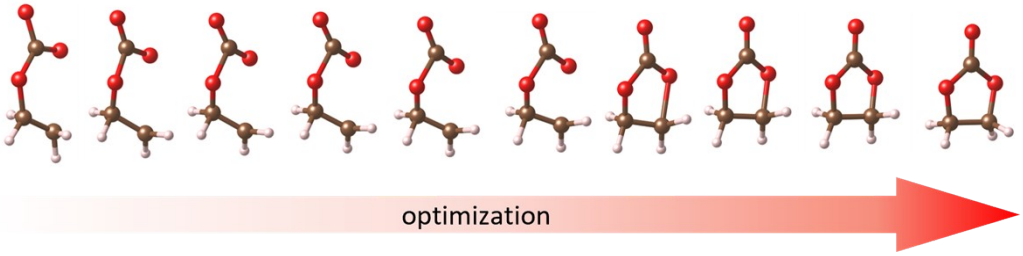

Figure S9 Structural optimization process of the ring-opened state of isolated EC.

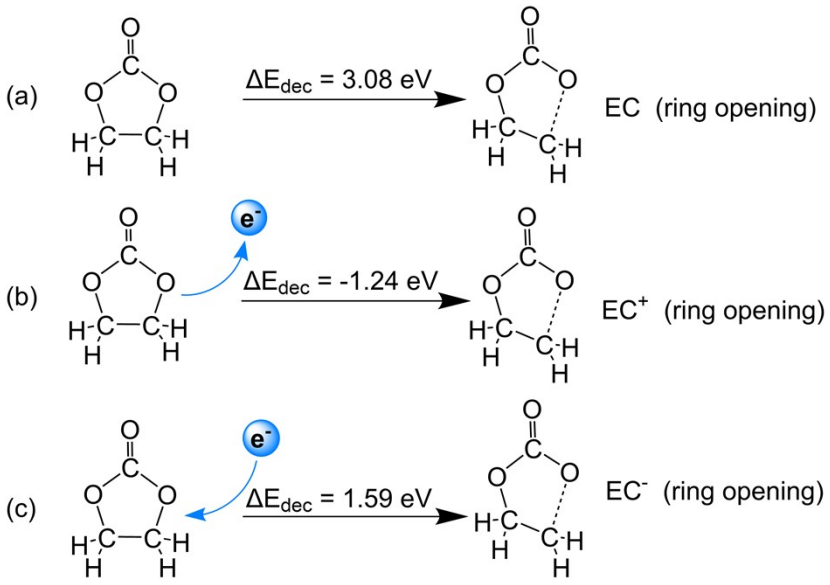

Figure S10 The decomposition energy of isolated EC in three scenarios: pristine (neutral) (a), losing one electron (b), and gaining one electron (c).

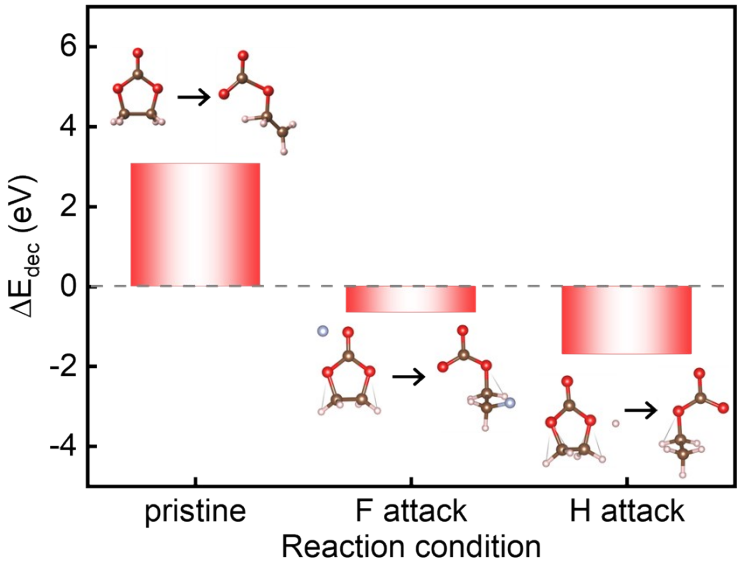

Figure S11 Decomposition energy of the ring-opening reaction of EC under F and H attack.

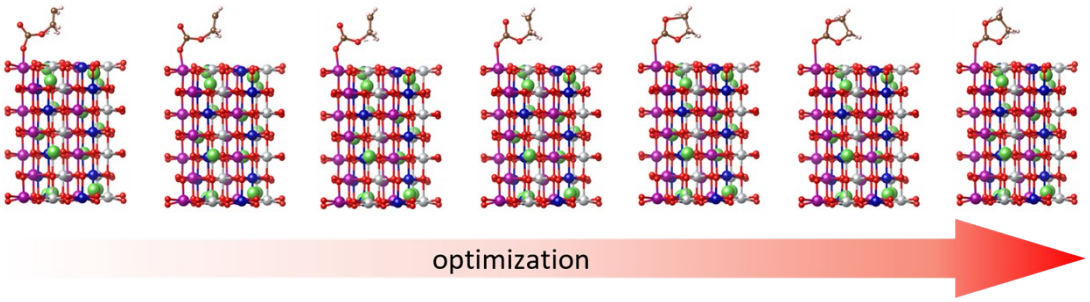

Figure S12 Structural optimization process of the ring-opened state of EC on the $Li_{1/3}NCMO$ surface.

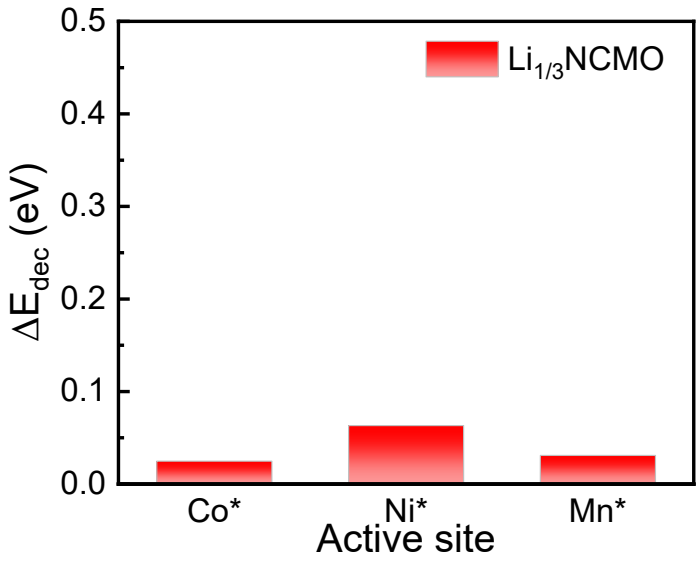

Figure S13 Decomposition energy of the CO_2 release reaction of EC on Ni, Co, and Mn sites of $Li_{1/3}NCMO$ surface.

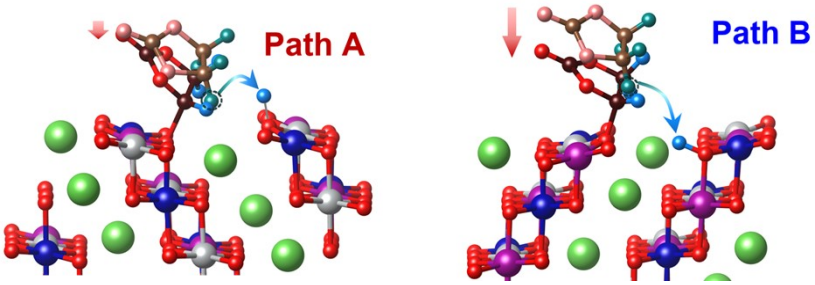

Figure S14 Schematic diagram of direct dehydrogenation reactions of EC on the $Li_{1/3}$NCMO surface.

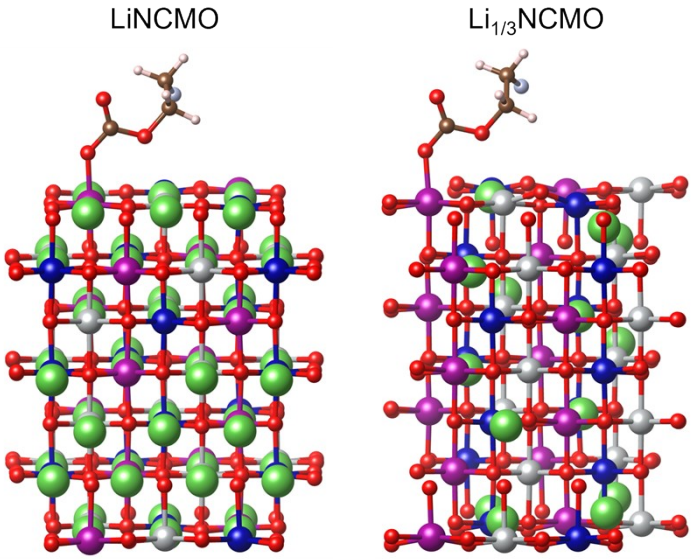

Figure S15 Schematic diagram of EC on LiNCMO and $Li_{1/3}$NCMO surfaces in the presence of F atom.

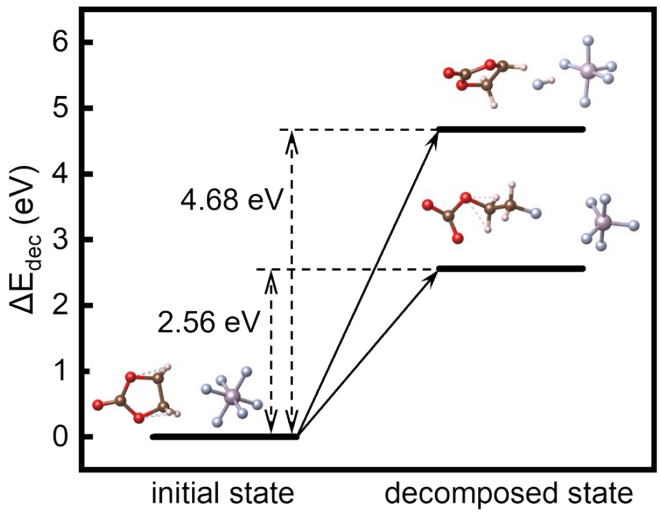

Figure S16 Decomposition energies for the F-assisted dehydrogenation reaction and F-assisted ring-opening reaction of EC in the presence of PF_6^- without cathode.

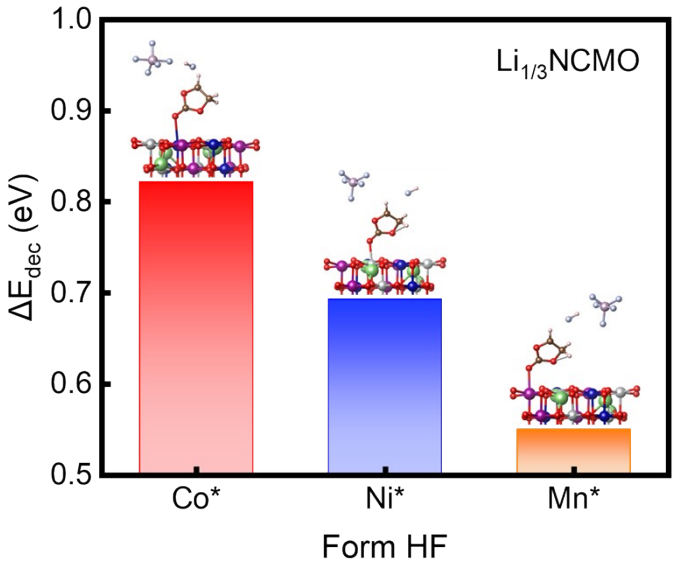

Figure S17 Decomposition energy of F-assisted dehydrogenation reactions of EC on Co, Ni, and Mn sites of $Li_{1/3}NCMO$ surface in the presence of PF_6^-.

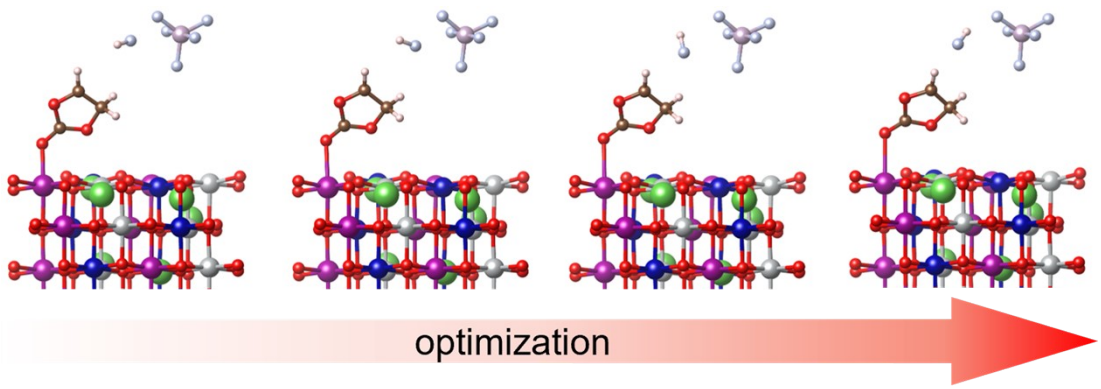

Figure S18 Structural optimization process of HF rotation after F-assisted dehydrogenation reaction of EC on $Li_{1/3}$NCMO.

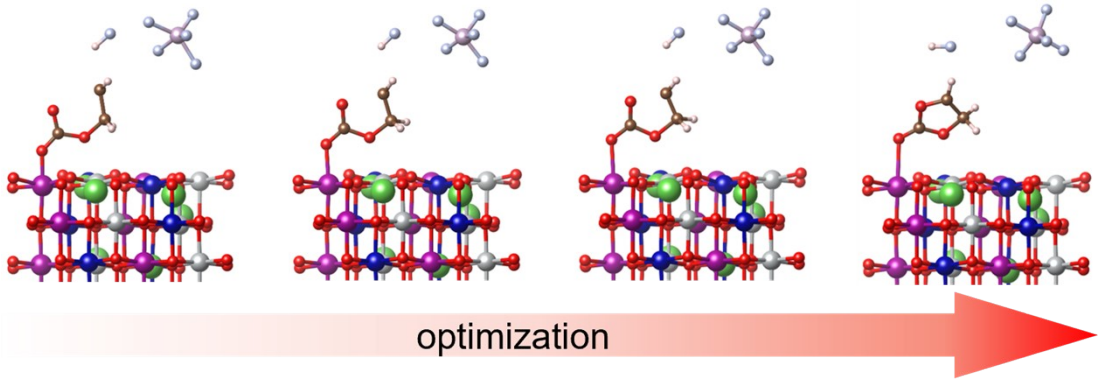

Figure S19 Structural optimization process of EC ring-opened state after F-assisted dehydrogenation reaction on $Li_{1/3}$NCMO.

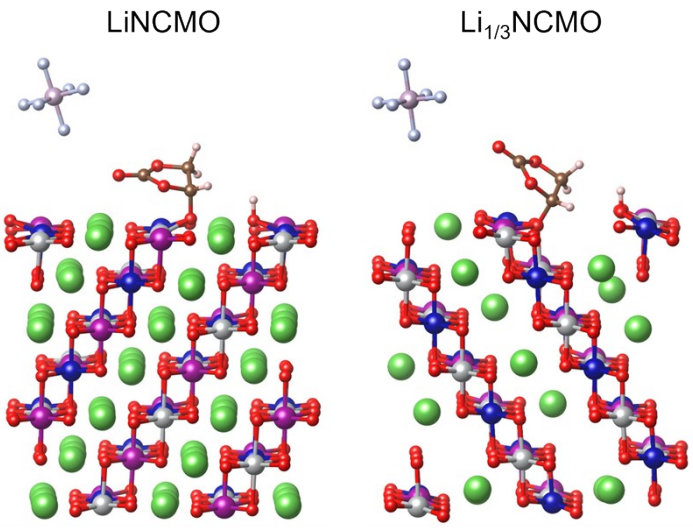

Figure S20 Structural schematic diagram of the direct dehydrogenation reactions of EC on LiNCMO and $Li_{1/3}$NCMO surfaces in the presence of PF_6^-.

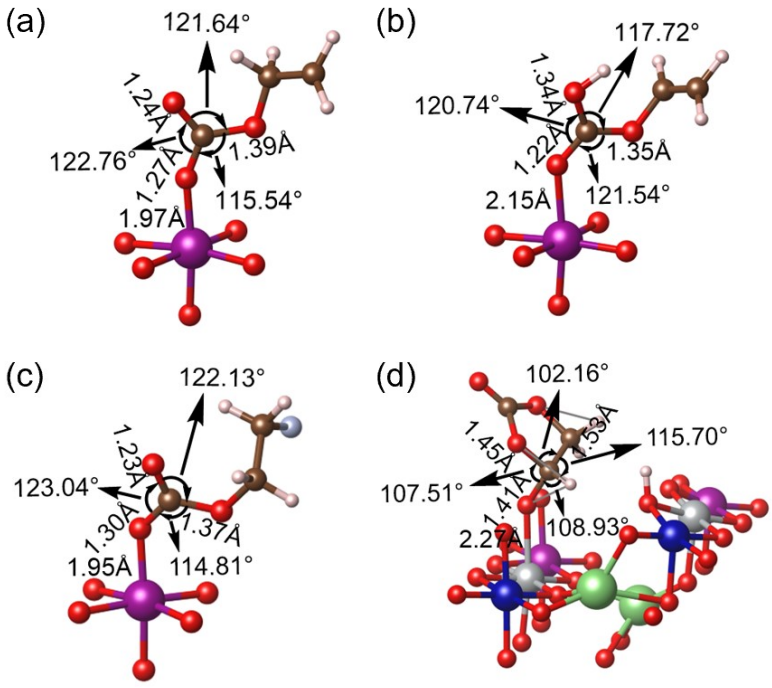

Figure S21 Geometric structure of the final states for the direct ring-opening reaction (a), H-transfer-assisted ring-opening reaction (b), F-assisted ring-opening reaction (c), and direct dehydrogenation reaction (d) of the EC on the $Li_{1/3}$NCMO surface.

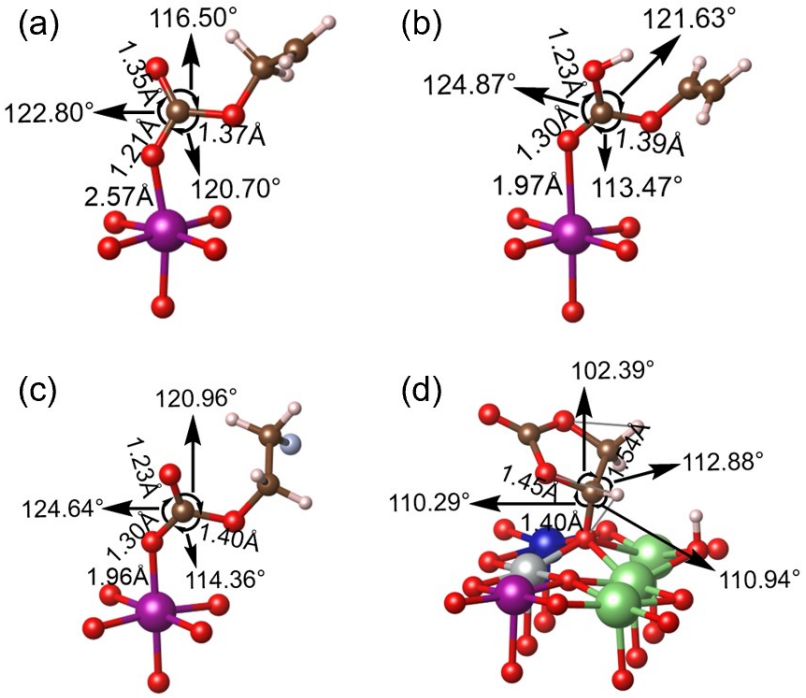

Figure S22 Geometric structure of the final states for the direct ring-opening reaction (a), H-transfer-assisted ring-opening reaction (b), F-assisted ring-opening reaction (c), and direct dehydrogenation reaction (d) of the EC on the LiNCMO surface.

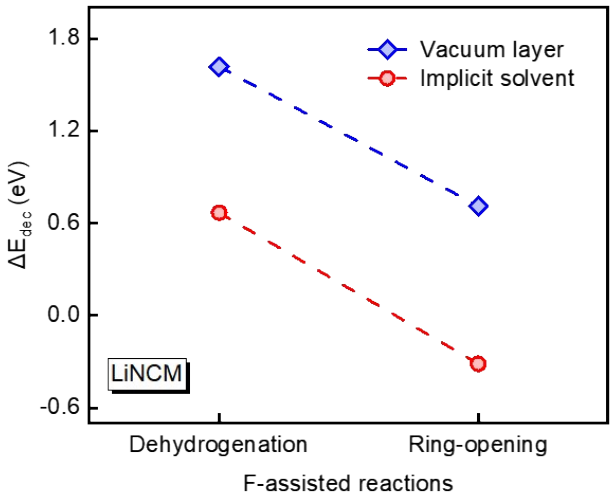

Figure S23 Decomposition energies of EC and PF_6^- in F-assisted dehydrogenation and ring-opening reactions on the LiNCMO cathode surface under vacuum versus implicit solvent conditions.

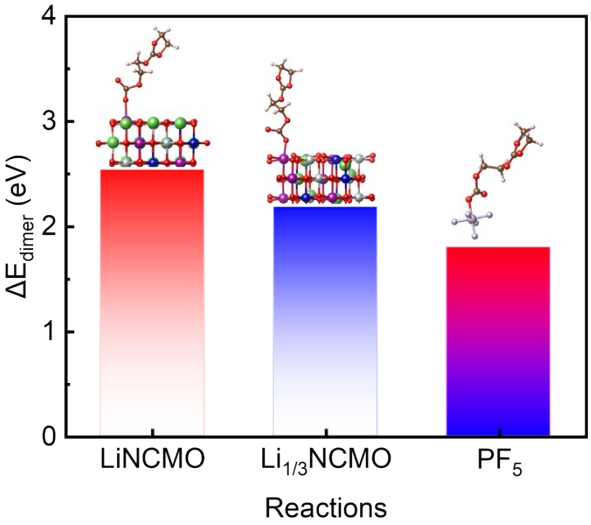

Figure S24 The dimerization energy ($^{\Delta E_{dimer}}$) of EC on the LiNCMO surface, $Li_{1/3}NCMO$ surface, and PF_5 (EC carbonyl oxygen combines with the transition metal on two cathode surfaces).

Table S5 The decomposition energies (ΔE_{dec}) and activation barriers (E_a) of all decomposition reactions of EC and EC with PF_6^-.

	Without cathode	**LiNCMO**	**$Li_{1/3}$NCMO**
Direct ring-opening reaction	×	×	×
H-transfer-assisted ring-opening reaction	ΔE_{dec}=0.58eV E_a=3.01eV	ΔE_{dec}=0.79eV E_a=4.20eV	ΔE_{dec}=0.69eV E_a=3.08eV
CO_2 release reaction	ΔE_{dec}=-0.42eV E_a=2.98eV	ΔE_{dec}=0.21eV E_a=3.14eV	ΔE_{dec}=0.21eV E_a=2.61eV
Direct dehydrogenation reaction	—	ΔE_{dec}=-0.57eV E_a=4.84eV	ΔE_{dec}=-2.71eV E_a=0.15eV
F-assisted ring-opening reaction	ΔE_{dec}=2.56eV	ΔE_{dec}=0.71eV E_a=1.64eV	ΔE_{dec}=0.61eV E_a=1.38eV
F-assisted dehydrogenation reaction	ΔE_{dec}=4.68eV	ΔE_{dec}=1.62eV E_a=2.43eV	ΔE_{dec}=0.55eV E_a=1.56eV
F-assisted CO_2 release reaction	ΔE_{dec}=-0.02eV	ΔE_{dec}=0.43eV E_a=2.94eV	ΔE_{dec}=0.39eV E_a=2.35eV
F-assisted direct dehydrogenation reaction	—	ΔE_{dec}=0.28eV	ΔE_{dec}=-1.32eV
Polymerization reaction	ΔE_{dimer}=1.80eV	ΔE_{dimer}=1.89eV	ΔE_{dimer}=0.93eV